Electronic Supplementary Information (ESI)

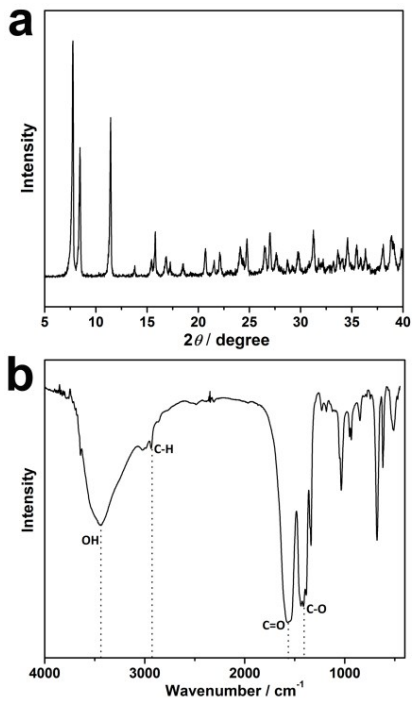

Fig. S1 (a) XRD pattern of the Ni-Mn precursors, (b) FTIR spectra of the Ni-Mn precursors.

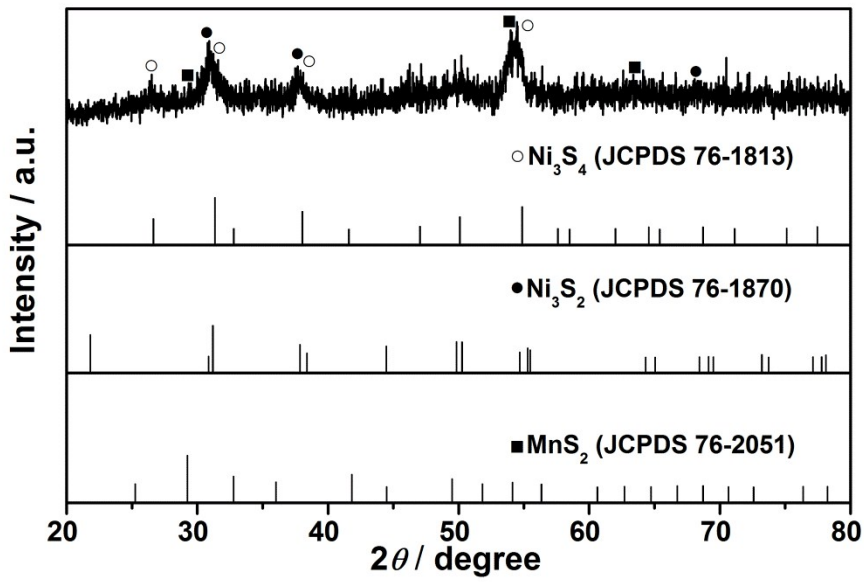

Fig. S2 XRD patterns of the synthesized hollow ellipsoids Ni-Mn sulfides.

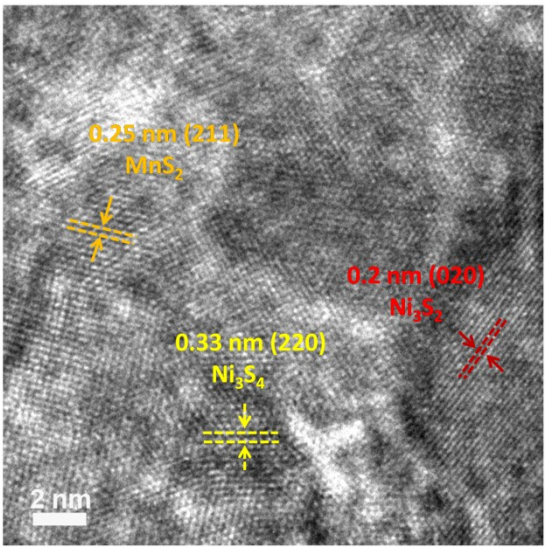

Fig. S3 High-resolution TEM image of the hollow ellipsoids Ni-Mn sulfides.

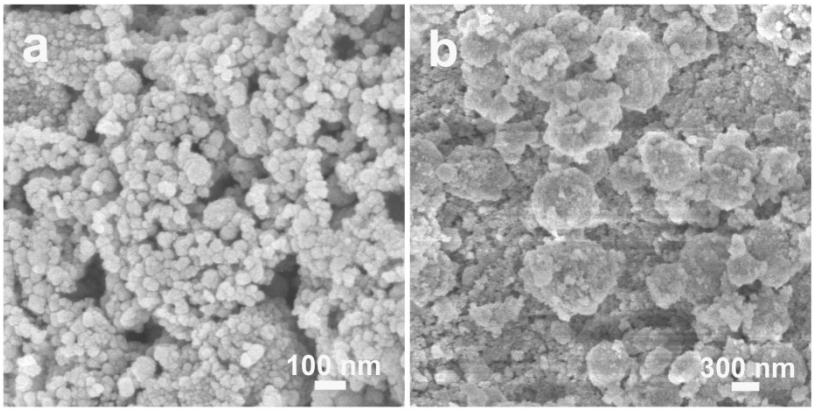

Fig. S4 SEM images of the nickel sulfide (a) and manganese sulfide (b).

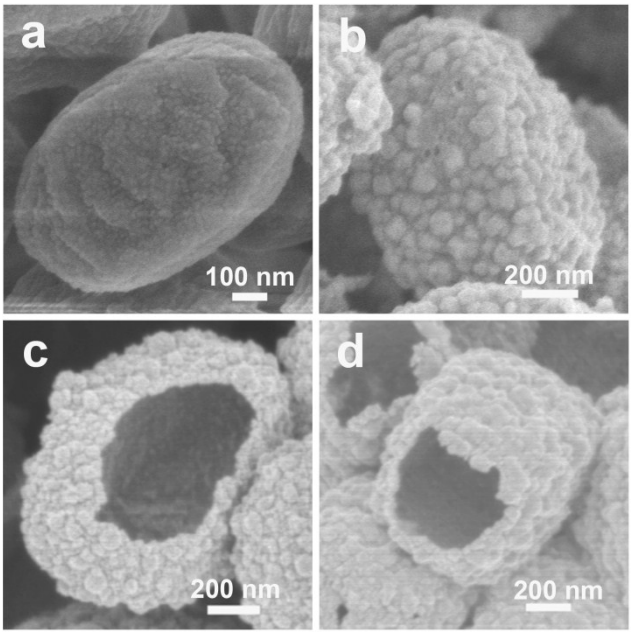

Fig. S5 Products obtained after sulfidation of the solid ellipsoids Ni-Mn precursors at 120 °C for different durations: (a) 30min, (b) 50 min, (c) 80 min, (d) 120 min.

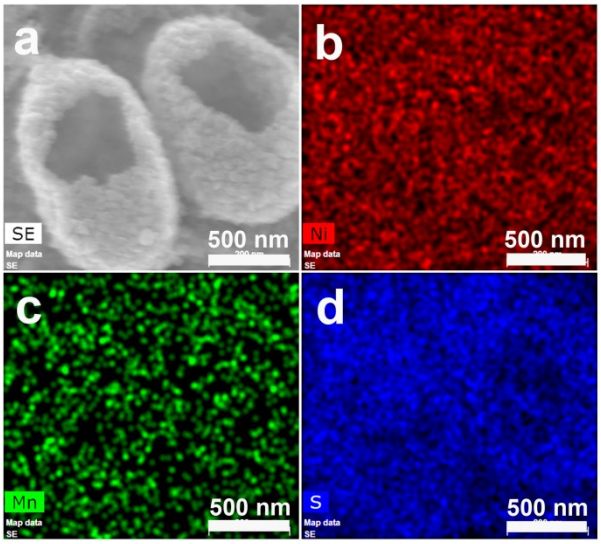

Fig. S6 (a) FESEM image of hollow ellipsoids Ni-Mn sulfides and corresponding elemental mapping images: (b) Ni, (c) Mn and (d) S.

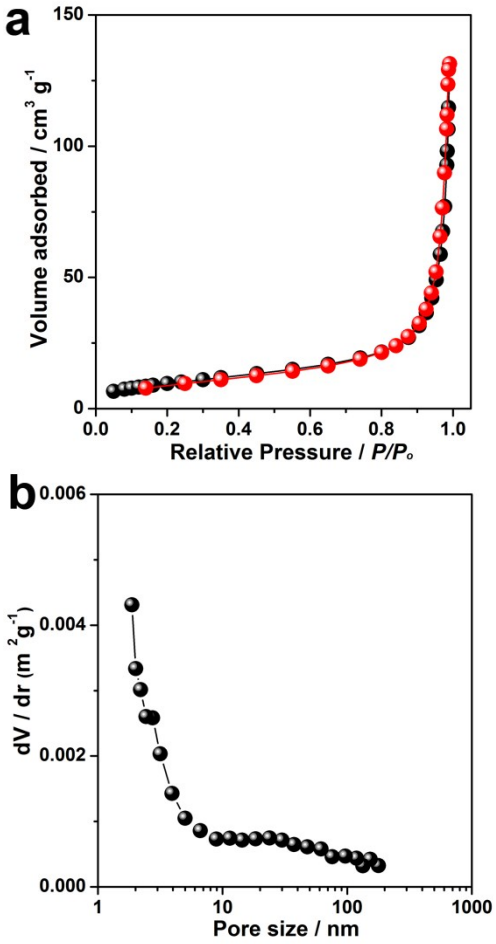

Fig. S7 (a) the N_2 adsorption-desorption isotherm and (b) pore size distribution of hollow ellipsoids Ni-Mn sulfides.

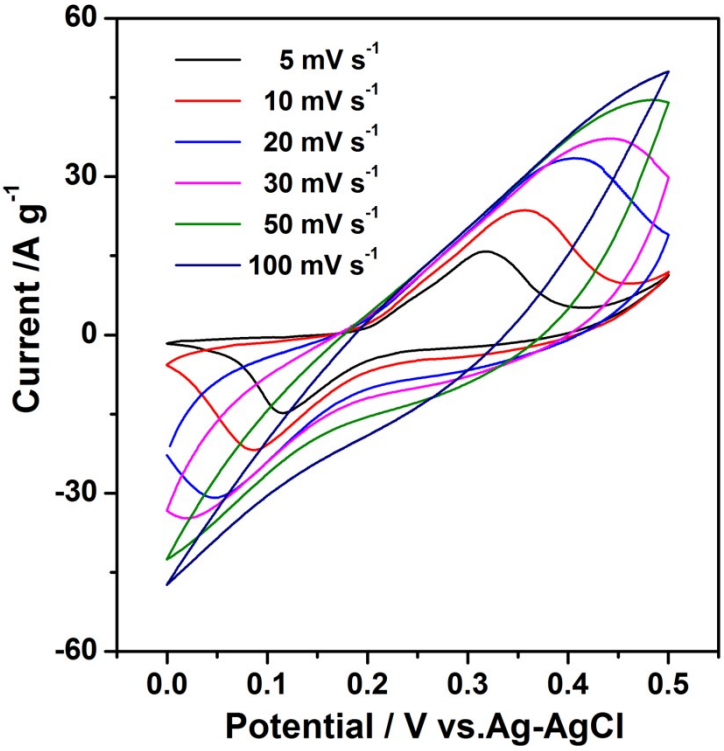

Fig. S8 CV curves of hollow ellipsoids Ni-Mn sulfides at different scan rates.

Table.S1 Comparison specific capacitances of hollow ellipsoids Ni-Mn sulfides with other hybrid metal oxides/sulfides.

Electrode materials	Specific capacitance	References
ZnO-NiO hollow spheres	497 F g^{-1} at 1.3 A g^{-1}	60
Co_3O_4/CeO_2 nanowire arrays	1037.5 F g^{-1} at 2.0 A g^{-1}	61
Hollow spiny Ni-Mn oxides	1140F g^{-1} at 1.0 A g^{-1}	62
Co-Ni-Mn oxide nanowires	554 F g^{-1} at 2.0 A g^{-1}	63
Hierarchical $NiCo_2O_4$	816 F g^{-1} at 2.0 A g^{-1}	64
Mn-Ni-Co oxide nanowires	638 F g^{-1} at 1.0 A g^{-1}	65
ZnO@ZnS core-shell arrays	603.8 F g^{-1} at 2.0 A g^{-1}	66
ZnS-NiS_2 hollow spheres	970 F g^{-1} at 2.0 A g^{-1}	67
$NiCo_2S_4/Co_9S_8$ hollow spindles	749 F g^{-1} at 4.0 A g^{-1}	68
Ni_2CoS_4 nanoboxes	1200 F g^{-1} at 2.0 A g^{-1}	69
3D hierarchical Ni-Co sulfides	276.7 F g^{-1} at 0.5 A g^{-1}	70
Hedgehog-like hollow Ni-Mn sulfides	1176 F g^{-1} at 2.0 A g^{-1}	40
Hollow ellipsoids Ni-Mn sulfides	1636.8 F g^{-1} at 2.0 A g^{-1}	This work

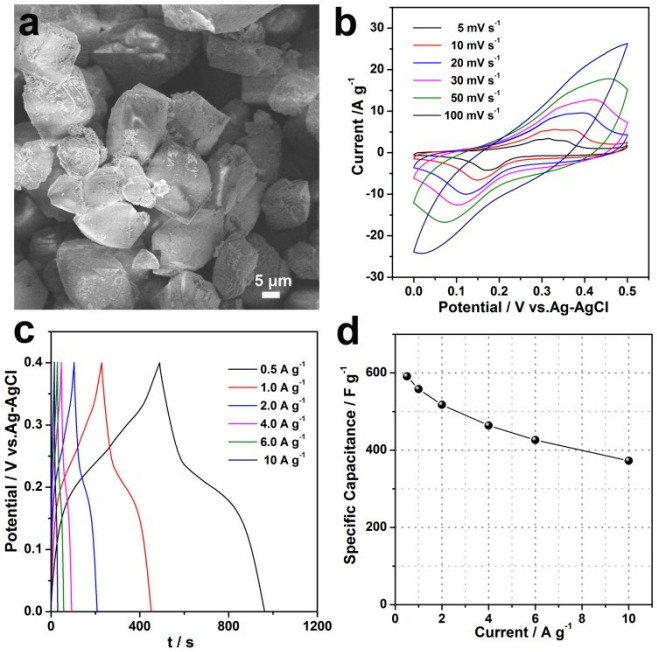

Fig. S9 (a) SEM image of the solid Ni-Mn sulfides, (b) CV curves at scanning rates from 5 to 100 mV s^{-1}, (c) CD curves at current densities from 0.5 to 10 A g^{-1}, (d) Specific capacitance at current densities from 0.5 to 10 A g^{-1}.

Table. S2 Performance comparison of the hollow ellipsoids Ni-Mn sulfides/GCE with other glucose sensors.

Sensing materials	Linear range (μM)	Detection limit (μM)	References
Honeycomb-like Ni@C composites	2-280	0.9	17
α-NiS hollow spheres	0.125-200	0.08	72
Lithium-doped NiO nanofibers	0.5-278	0.1	73
Copper oxide nanostructures	0.01-10	1.37	74
Reduced graphene oxide/ZnO	0.02-22.48	0.02	75
Nafion/Cu_2O	0.002-0.35	1.3	76
Hierarchically porous $NaCoPO_4$-Co_3O_4 hollow microspheres	1.0-26	0.125	77
Hollow ellipsoids Ni-Mn sulfides	0.05-500	0.02	This work

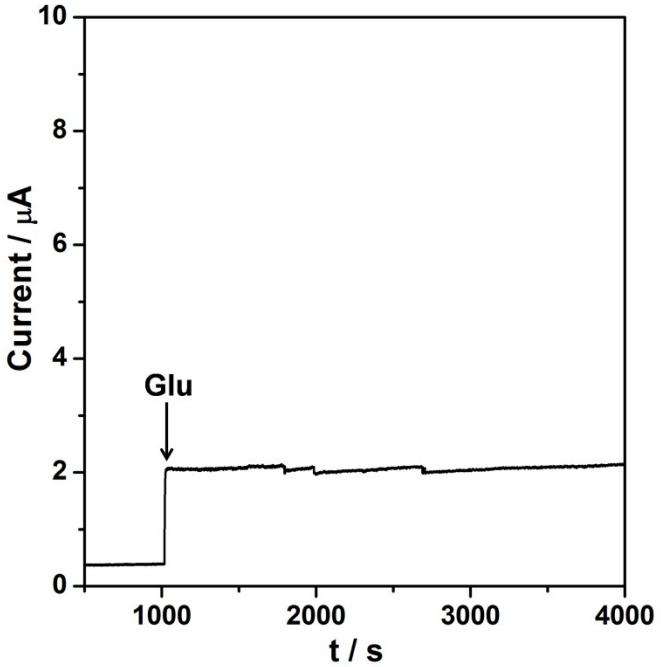

Fig. S10 The stability of the response current for hollow ellipsoids Ni-Mn sulfides/GCE sensors after the addition of 40 μM glucose.

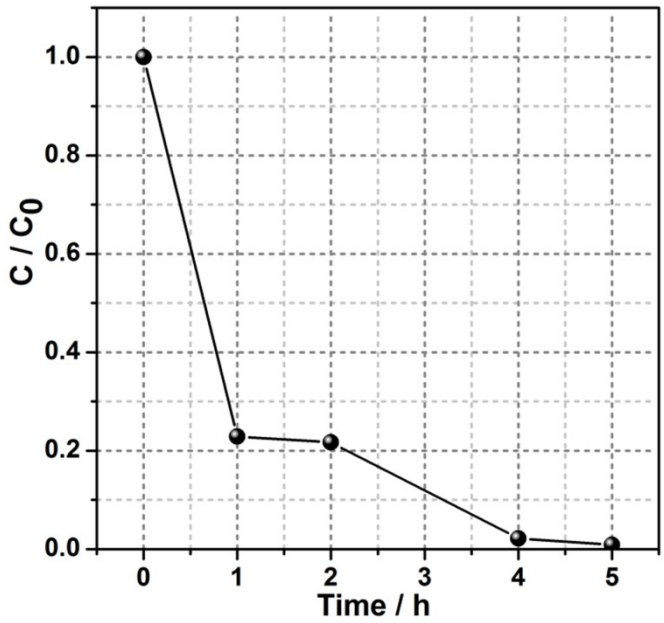

Fig. S11 Curves of the adsorption extent of Congo red as a function of contact time for hollow ellipsoids Ni-Mn sulfides.

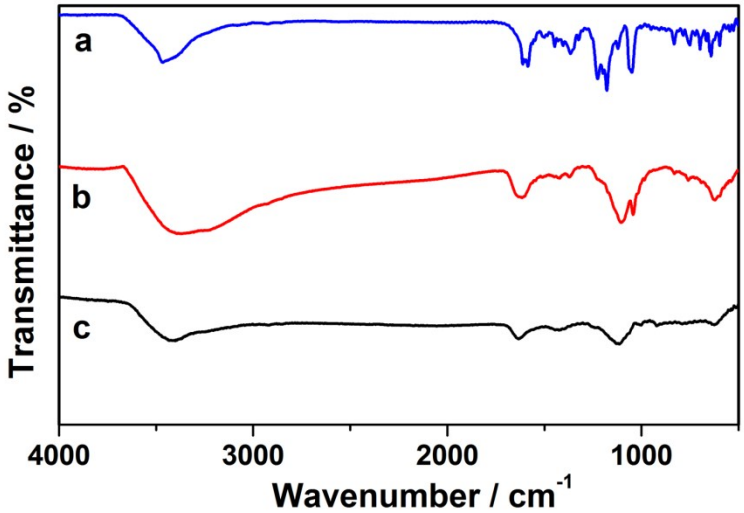

Fig. S12 IR spectra of Congo red (a), hollow ellipsoids Ni-Mn sulfides after water purification (b) and (c) hollow ellipsoids Ni-Mn sulfides.